Tribol Lett (2010) 39:63–69
DOI 10.1007/s11249-009-9567-7

ORIGINAL PAPER

Multiple Slips in Atomic-Scale Friction: An Indicator for the Lateral Contact Damping

Raphael Roth · Thilo Glatzel · Pascal Steiner · Enrico Gnecco · Alexis Baratoff · Ernst Meyer

Received: 10 July 2009 / Accepted: 23 December 2009 / Published online: 23 January 2010

Abstract The occurrence of multiple jumps in 2D atomic-scale friction measurements is used to quantify the viscous damping accompanying the stick–slip motion of a sharp tip in contact with a NaCl(001) surface. Multiple slips are observed without apparent wear for normal forces between 13 and 91 nN. For scans parallel to [100] directions, the tip jumps between minima of the substrate corrugation potential in a zigzag fashion. An algorithm is applied to determine histograms of lateral force jumps which characterize multiple slips. The same algorithm is used to classify multiple slips occurring in calculated lateral force maps. Comparisons between simulations and experiments indicate that the nanometer-sized contact is underdamped at intermediate loads (13–26 nN) and becomes slightly overdamped at higher loads. The proposed procedure is a novel way to estimate the lateral contact damping which plays an important role in the interpretation of measurements of the velocity and temperature dependence of friction, of slip duration, and of the reduction of friction by applied perpendicular or parallel oscillations.

Keywords Nanotribology · Energy conservation · Friction mechanisms · Stick–slip · AFM

R. Roth · T. Glatzel (✉) · P. Steiner · E. Gnecco · A. Baratoff · E. Meyer
Department of Physics, University of Basel, Klingelbergstr. 82, 4056 Basel, Switzerland
e-mail: thilo.glatzel@unibas.ch

E. Meyer
e-mail: ernst.meyer@unibas.ch

1 Introduction

Since the invention of the friction force microscope (FFM) [1], stick–slip movement was found to be characteristic for a sharp tip at the end of a cantilever which is moved perpendicular to its axis in soft contact with an atomically flat surface. Since the periodicity of the observed sawtooth-like lateral force pattern often corresponds to the spacing between adjacent unit cells, such experimental observations were readily associated with atomic stick–slip motion, where the tip slips between energetically favored neighboring lattice sites [1, 2]. Each slip is accompanied by a jump in the lateral force F_L at the corresponding position x_s of the cantilever support.

The 1D Tomlinson model [3] has often been used to interpret such atomic-scale friction phenomena. A particle representing the tip is dragged by an elastic spring of stiffness k_{eff} connected to a support moving at a constant velocity v over a sinusoidal potential of peak-to-peak amplitude E_0 and period a representing the surface. Note that k_{eff} accounts for the combined torsion of the cantilever and the contact shear. In contrast to earlier assumptions [4], recent atomic-scale FFM measurements on alkali halide surfaces at loads in the few nN range have shown that $k_{eff} \sim 1$ N/m is typically dominated by the lateral contact stiffness, so that the entities which are most deflected during each stick stage are the contacting atoms at the tip apex and at the sample surface rather than the cantilever [5, 6]. Atoms further away are also deflected sideways, albeit less because more atoms take up the stresses generated in the contact region. The net shear displacements in that region, in opposite directions at the apex and at the surface, can in principle exceed several lattice spacings but still remain elastic. During each slip, the energy stored in the preceding stick stage is released and carried away from the

contact. In the wearless regime realized at low loads, the stressed atoms return to their respective equilibrium positions on time scales which are long compared to typical periods of lattice vibrations, but almost instantaneous compared to the time required to scan over a surface unit cell. Actually, FFM experiments suggest that transfer of the softer material initially occurs until a regular stick–slip pattern is observed. This is confirmed by simulations on ionic crystals which show that the tip apex then adopts a "self-limited structure" at a given load [7]. As long as this structure remains relatively sharp, the tip deforms more than the sample, hence contributes more to the slip distance and to the accompanying energy dissipation. Asserting that the tip slips, as is often done for the sake of exposition, therefore also has a physical basis.

Within the Tomlinson model, slips over more than one lattice spacing a can in principle occur for a sufficiently strong corrugation amplitude E_0 and/or a sufficiently low k_{eff}. In the quasi-static limit, the number of minima in the total potential energy determines the *possible* landing points of the tip after a slip. The Tomlinson parameter $\eta = 2\pi^2 E_0/k_{\text{eff}}a^2$ can distinguish regimes where the tip is sliding smoothly ($\eta < 1$), executes stick–slip motion with single slips ($1 < \eta < 4.6$) or, possibly exhibits double slips ($4.6 < \eta < 7.79$) or even bigger multiple slips ($\eta > 7.79$). Whereas a few authors focused attention on the occurrence of single versus double slips as a function of additional parameters (contact damping, support velocity, temperature) [8–10], Medyanik et al. [11] derived the above-mentioned η threshold values from a simple analytic criterion. Most studies, however, assumed that the tip slips to the adjacent available energy minimum once the current minimum disappears as the support is slowly pulled past a critical position x_{sc} (mod a). This is justified if lateral contact vibrations are overdamped, owing to coupling to substrate (and/or tip) excitations, so that the energy released in each jump is dissipated quicker than the tip would cross a lattice spacing in the absence of damping. This inelastic coupling increases with decreasing tip-sample distance, just as for atoms or molecules adsorbed with different bond strengths on a clean surface [12]. One therefore expects the contact damping to increase with applied load, at least for dry friction of sub-nanometer-sized single-asperity contacts. Effects due to interface incommensurability, roughness, defects, or adsorbed species, which are especially relevant in wider area contacts [13, 14] are then likely not so important. Recent FFM measurements on graphite showed transitions from single to double and to triple slips with increasing load, in agreement with the above-mentioned threshold η values [11]. This is qualitatively in accordance with the near-independence of k_{eff} and the linear dependence of E_0 on the applied load previously measured on NaCl(001) in ultra-high vacuum (UHV) [5]. However, it is by no means obvious whether the increase in η with load should dominate over the expected increase in γ, as seems required to explain the transitions in question.

In dynamic extensions of the Tomlinson model [4, 8, 9, 15], an effective tip or contact mass m and damping coefficient γ are introduced in the equation of motion for the tip in contact, thus making the prediction of multiple slips more realistic. Since some fraction of the tip kinetic energy is lost during each jump due to nonzero damping, not all energy minima can be reached. Thus, the number of possible slips calculated from η alone must be considered as an upper limit which may be achieved in the strongly underdamped case. In the opposite case, multiple jumps become suppressed, as mentioned earlier. Thus, the occurrence of multiple slips and the lateral contact damping are intimately connected. This study provides a novel way to estimate γ relative to a critical value which distinguishes overdamped from underdamped contacts. The lateral contact damping plays an important role in the interpretation of FFM measurements of the velocity and temperature dependence of friction [16, 17], of slip duration [18], and of the reduction of friction by applied perpendicular [19, 20] or parallel oscillations [21].

Direct estimates of γ have so far been obtained in a few situations where a viscous contribution to the average friction proportional to the support velocity could be detected. Thus, Bilas et al. [22] found $\gamma \approx 10^{-5}$ kg s^{-1} $\sim 5\gamma_c$ for an FFM tip scanning on $NbSe_2$ in air by comparing measured velocity-dependent friction curves with simulated ones. The damping was attributed to viscous drag by adsorbed water. At low scan velocities and loads, regular single slips were observed, consistent with overdamping. Yabing et al. [23] estimated $\gamma \approx 5 \times 10^{-6}$ kg s^{-1} for a voltage-dependent contribution to the friction of oxidized highly n-doped GaAs forward-biased by means of a platinum-coated tip in UHV conditions. They associated the small excess friction with electric coupling to slowly relaxing trapped charges in the oxide. Reinstädtler et al. [24] obtained $\gamma \approx 10^{-6}$ kg s^{-1} from the measured quality factor in air of the torsional resonance of a cantilever in contact with an oxidized silicon sample driven by ultrasonic shear waves under ambient conditions. The contact was described by a lateral stiffness and damping coefficient, but zero inertial mass.

In all those cases, the contacts had estimated radii of several nanometers and therefore encompassed many atoms. The measured load dependence of the average friction, assumed proportional to the contact area was well described by continuum elasticity models. The proportionality constant (shear strength) roughly plays the same role as the slope of E_0 versus load, although no site-dependent corrugation potential enters such models. Their applicability has recently been questioned on the basis of

large-scale atomistic simulations [14] which reveal that multiple contacts are formed and broken even for nominal contact radii of several nanometers.

An absolute determination of contact damping from atomically resolved FFM measurements appears impossible because scan velocities are orders of magnitude lower than those required to directly detect the viscous friction force $-\gamma v$. The interpretation of such measurements relies on uncertain assumptions about the contact mass or the angular frequency $\omega_x = \sqrt{(k_{\mathrm{eff}}/m)}$ of lateral contact vibrations, the damping rate $\Gamma = \gamma/m$ or the ratio Γ/Γ_c, $\Gamma_c = 2\omega_x$ being the critical damping rate. In particular, identifying m with the mass of the whole tip, ω_x with the torsional resonances frequency of the cantilever in contact or Γ with the full width at half-maximum of the corresponding spectral peak is unfortunately not justified for atomic-scale contacts [18].

2 One-Dimensional Model

In order to illustrate how damped dynamics determines the landing point of the tip, we display in Fig. 1 the potential profile $U(x)$ (surface corrugation + energy stored in the spring) at the onset of a slip together with the variation of the tip (kinetic + potential) energy during the slip event for two values of the relative damping γ/γ_c. For the sake of simplicity, the calculations are performed within the 1D Tomlinson model without thermal activation.

During the preceding stick stage, the tip is located in a potential minimum satisfying the mechanical equilibrium

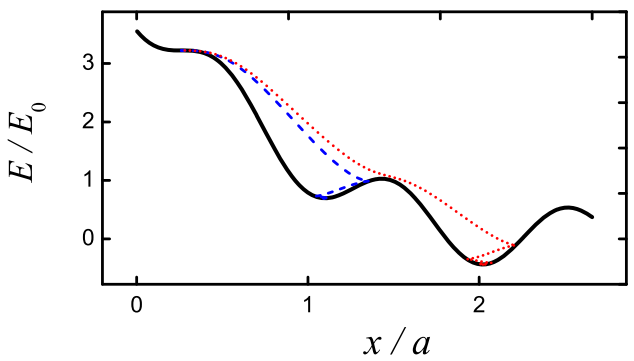

Fig. 1 Variation of the total energy E during a slip event versus the instantaneous tip coordinate x (in units of the corrugation amplitude E_0 and the lattice spacing a) calculated for two values of the damping ratio: $\gamma/\gamma_c = 1$ (*dashed blue curve*) and $\gamma/\gamma_c = 0.8$ (*dotted red curve*). The potential energy U (*solid black line*) at the onset of the slip is shown for comparison. For the assumed value $\eta = 12.8$, slips of up to $4a$ are in principle allowed [11], but only a and $2a$ slips are realized in the two illustrated cases

condition $\mathrm{d}U/\mathrm{d}x = 0$. This adiabatic approximation holds as long as the support velocity v is low so that slips occur much faster than the time to move over one lattice spacing a. The slip is initiated at the tip position x_c where in addition the equilibrium becomes unstable, i.e., $d^2U/\mathrm{d}x^2 = 0$. For the chosen value $\eta = 12.8$, the instability occurs at $x_c/a = 0.2645$ when the support is at $x_{sc}/a = 2.2934$. In both cases shown, the tip executes oscillations, i.e., its dynamics is underdamped in the potential well where it is trapped. A particular well is selected if the energy reduced by damping during the initial tip swing drops below the nearest blocking potential maximum. The damping range allowing double slips and the corresponding values for larger multiple slips are therefore determined by the overall potential landscape. Nevertheless, referring those values to the critical damping $\gamma_c = 2\sqrt{(k_{\mathrm{eff}}m)}$ defined by the oscillation frequency of the harmonic spring potential is justified not only by computational convenience, but also by the physics of the problem. Indeed, multiple slips can only occur for relatively high values of η. On the one hand, the spring extension just before a slip is then $(x_{sc} - x_c) \approx \pi E_0/(k_{\mathrm{eff}}a)$ [5], and contributes almost exclusively to the stored potential energy. On the other hand, the potential energy after completion of as slip to the lowest well (around $x = x_{sc}$) is nearly $-E_0/2$. Therefore, the energy released and dissipated during such a slip is approximately

$$\Delta E_{\max} \sim \frac{k_{\mathrm{eff}}(x_{sc} - x_c)^2}{2} + \frac{E_0}{2} = \left(\frac{\eta}{2} + 1\right)\frac{E_0}{2}, \qquad (1)$$

hence is dominated by the first, harmonic spring term. For $\eta = 12.8$, Eq. 1 predicts $\Delta E_{\max} = 3.7E_0$, which is remarkably close to the calculated value for the double slip illustrated in Fig. 1. In accordance with this conclusion, this figure, and similar plots for other values of γ/γ_c (data not shown), illustrates that during most of the "slip time," the modulation of the total potential by the surface corrugation has a relatively small influence on the "total energy trajectory" which ends up in the lowest well. Thus, although for large η the curvatures at the minima of the corrugation potential are higher than k_{eff}, the critical damping for the energetically most favorable slips is largely determined by k_{eff}. Note finally that at a finite temperature slips can be prematurely activated over the energy barrier which vanishes when $x_s = x_{sc}$ [16, 17, 25]. As a consequence of the underlying probability distribution of initial tip positions and velocities, slips of different lengths can randomly occur along single scan lines around the above-mentioned η threshold values in the underdamped case. This has been observed in previous simulations [8, 9, 10] and experiments [11], as well as in this study (see Fig. 4).

3 Method

In this article, we present and analyze room temperature lateral force measurements performed over a NaCl(001) substrate in UHV for a wider range of applied loads than hitherto studied in our group [5]. As shown in that study, the amplitude of the tip-sample corrugation potential is a linear function of the applied load. One can therefore control the parameter η, which can in turn be experimentally determined from $\eta = \frac{2\pi F_{\mathrm{L}}^{\max}}{k_{\mathrm{exp}} a} - 1$, where $F_{\mathrm{L}}^{\max}$ is the maximal lateral force experienced by the tip, $a = 0.564$ nm is the lattice spacing of NaCl, k_{exp} is the slope of the stick part of the lateral force versus support displacement, itself connected to the effective stiffness via $k_{\mathrm{eff}} = \frac{\eta+1}{\eta} k_{\mathrm{exp}}$ [5, 6].

As illustrated in Fig. 2, for scans along ⟨100⟩ directions parallel to the (001) cleavage surface of rocksalt-type crystals, previous FFM simulations in two dimensions [15, 20], as well as those discussed below, show that the tip slips over saddle points connecting adjacent minima of the corrugation potential, at least for η values not close to 1. As a consequence, the double and quadruple slips illustrated in Fig. 2 correspond to the single and double slips discussed in Sect. 2.

A sorting algorithm was applied to both experimental and computed lateral force data in order to classify slip-events according to the magnitude ΔF_{L} of particular jumps and thus to distinguish among single, double, triple, or quadruple slips.

The dynamic 2D Tomlinson model used to interpret our experimental room temperature data is based on coupled Langevin equations for the x and y tip coordinates, namely

$$m\frac{\mathrm{d}^2x}{\mathrm{d}t^2} + \gamma\frac{\mathrm{d}x}{\mathrm{d}t} + \frac{\partial U_{\mathrm{int}}(x,y)}{\partial x} = \xi(t), \tag{2}$$

and similarly for y, where m is the effective mass of the tip in contact, γ its lateral damping coefficient, and $\xi(t)$ a stochastic term proportional to γ according to the fluctuation–dissipation theorem [16, 17]. In accordance with the discussion of Eq. 1, critical damping is defined by $\gamma_c = 2\sqrt{k_{\mathrm{eff}} m_{\mathrm{tip}}}$. Referring γ to γ_{c} makes the analysis independent of the effective mass, which is not accurately known. For computational convenience, we set $m = 10^{-12}$ kg; this choice enables efficient computations on a PC with a time step which allows a fine sampling of the fast tip motion during slips.

The interaction potential $U_{\mathrm{int}}(x, y)$ is represented by the lowest Fourier component of the rocksalt lattice for the corrugation part and by an isotropic harmonic spring term, as recently justified by a comparison of calculated and measured lateral force maps on the same system [20]

$$U_{\mathrm{int}}(x,y) = -\frac{E_0}{2}\left[\cos\left(\frac{2\pi x}{a}\right)\cdot\cos\left(\frac{2\pi y}{a}\right)\right] + \frac{1}{2}k_{\mathrm{eff}}(x - x_{\mathrm{s}})^2, \tag{3}$$

where $x_{\mathrm{s}} = vt$ is the position of the support uniformly scanned along a [100] scan line specified by y. These coupled equations were solved numerically using Ermak's algorithm [27]. Two-dimensional lateral force maps were generated [20] using realistic parameters (v, E_0, k_{eff}, T) corresponding to previous measurements on the same system [5]. Simulations were done for a range of damping coefficients on both sides of γ_{c}. By comparing the resulting histograms of ΔF_{L} from experiment and theory, an estimation of $\gamma/\gamma_{\mathrm{c}}$ can be made for different loads, an aspect barely discussed in the literature, although it quite important in the field of nanotribology.

4 Experimental Setup

The measurements have been performed at room temperature in a home-built FFM operated in a UHV-environment with a pressure $p < 1 \times 10^{-10}$ mbar [28]. The deflection of a laser beam focused on the very end of the cantilever is tracked via a 4-quadrant photodiode (beam deflection

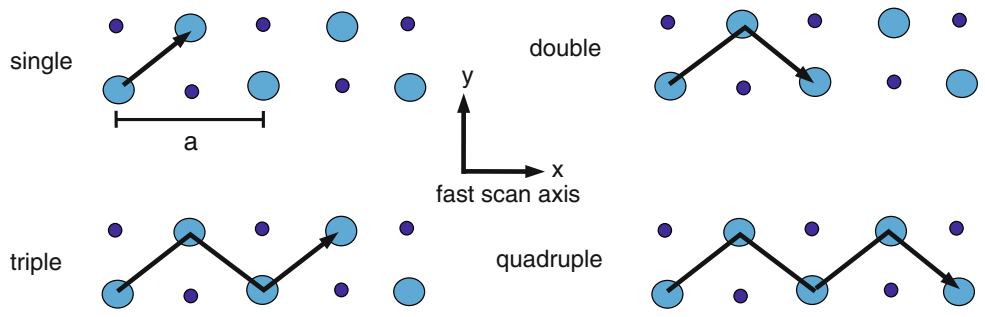

Fig. 2 Schematic illustration of the path of the tip while scanning along the [100] direction of a rocksalt (001) surface. The tip jumps from one minima to the next one in a zigzag fashion in steps of $a/2$, which is the distance between two consecutive minima of the 2D corrugation potential projected on the scan direction. Whether the Na^+- or the Cl^--sublattice correspond to the potential minima depends on the unknown nature and structure of the tip apex [26]

method). The vertical deflection of the beam is proportional to the normal force, whereas the horizontal deflection is proportional to the component of the lateral force along the fast scan direction (perpendicular to the cantilever axis).

The (001) surface of an in situ cleaved NaCl crystal was used as the sample. To remove surface charges created during the cleavage process, the crystal was heated up to 140 °C for 30 min in UHV. Rectangular silicon cantilevers with spring constants of $k_N = 0.097$ N/m for normal bending and $k_T = 64$ N/m for torsion were used. Elastic thin beam theory was applied to determine those stiffness, while for the sensitivity calibration of the beam-deflection setup the procedure described in [29] was used. Normal loads varying between 13 and 91 nN were applied to the cantilever, which was scanned at a velocity of 13 nm s^{-1} parallel to the [100] direction of the surface. Above this range, wear processes set in. All normal forces are defined with respect to the unbent cantilever (i.e., without adding adhesion forces).

5 Results and Discussion

As in previous 2D simulations of scans along the [100] direction [15], the tip exhibits regular zigzag slips between adjacent corrugation energy minima in the overdamped case.

In the underdamped case, multiple jumps of the type sketched in Fig. 2 appeared as η was successively increased, although no sharp threshold values could be identified at room temperature. The force variation during a n-tuple jump is then given by $n \times a/2 \times k_{\text{eff}}$. Note that for all values of $\eta > 1$, double slips occurred when the path of the support is very close to the atomic rows. As discussed in Sect. 3, they correspond to single slips by a in the 1D Tomlinson model. If the time resolution of the calculated friction maps is rather low, it is not possible to distinguish between two very fast consecutive $a/2$ jumps and a direct jump by a. For a realistic comparison, the same time and spatial resolutions were set in both experiment and simulations. However, the resulting artifacts do not affect our general conclusions.

By adjusting the damping γ in the range of $0.1 - 10 \cdot \gamma_c$, an upper limit for the damping can be estimated. For $\eta = 12.8$, the calculated histograms which show the onset of multiple slips are shown in Fig. 3. Solutions of Eqs. 2–3 for fixed x_s (i.e., assuming that support motion during a slip can be neglected) only depend on the dimensionless parameters $\eta, E_0/k_BT$, and Γ/ω_x, ω_x being the angular frequency of some characteristic vibration of the model. With our choice $\omega_x = \sqrt{(k_{\text{eff}}/m)}$ and the definition $\Gamma_c = 2\omega_x$ appropriate for a damped harmonic oscillator, energetically most favored multiple jumps for a given η appear in distributions like those

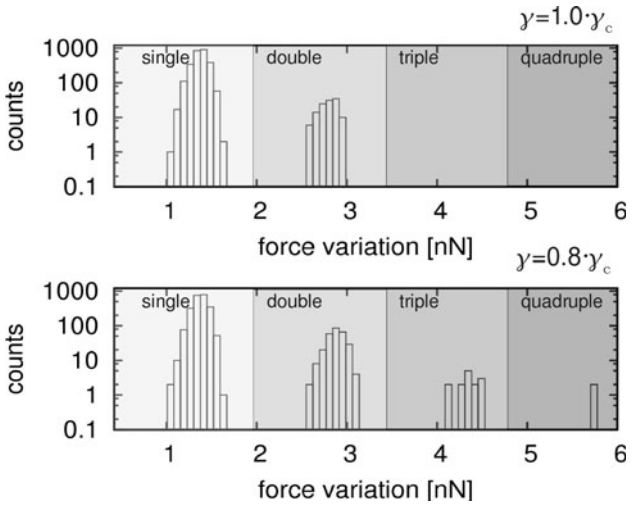

Fig. 3 Room temperature histograms of force jumps calculated for $\eta = 12.8$ for two representative values of the relative damping. The upper graph shows the distribution for $\gamma = 1.0 \cdot \gamma_c$ where only single and double slips are identified. The lower histogram is the result of a simulation with $\gamma = 0.8 \cdot \gamma_c$ where triple and quadruple slips are manifest

shown in Fig. 3 once γ becomes slightly undercritical. This consequence of the discussion in Sect. 2 provides a simple criterion to estimate the ratio γ/γ_c from jump histograms obtained from FFM measurements.

Figure 4 shows an example of the coexistence of different force jumps ΔF_L in an experimental scan. For the five values of the normal load that have been thoroughly analyzed, namely 13, 26, 39, 78, and 91 nN, the corresponding values of k_{eff} only varied in the range of 5.2 and 5.9 N/m. *This is consistent with a contact encompassing just a few atoms*. The amplitude E_0 of the corrugation potential was extracted from the measured maximum lateral force F_{max} versus load [5] and subsequently increased by 25% in order to roughly account for thermal activation

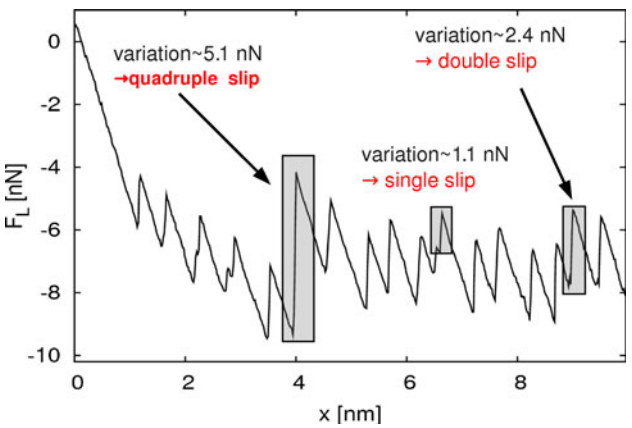

Fig. 4 Experimental lateral force trace taken at 91 nN normal load showing different types of jumps within one scan line

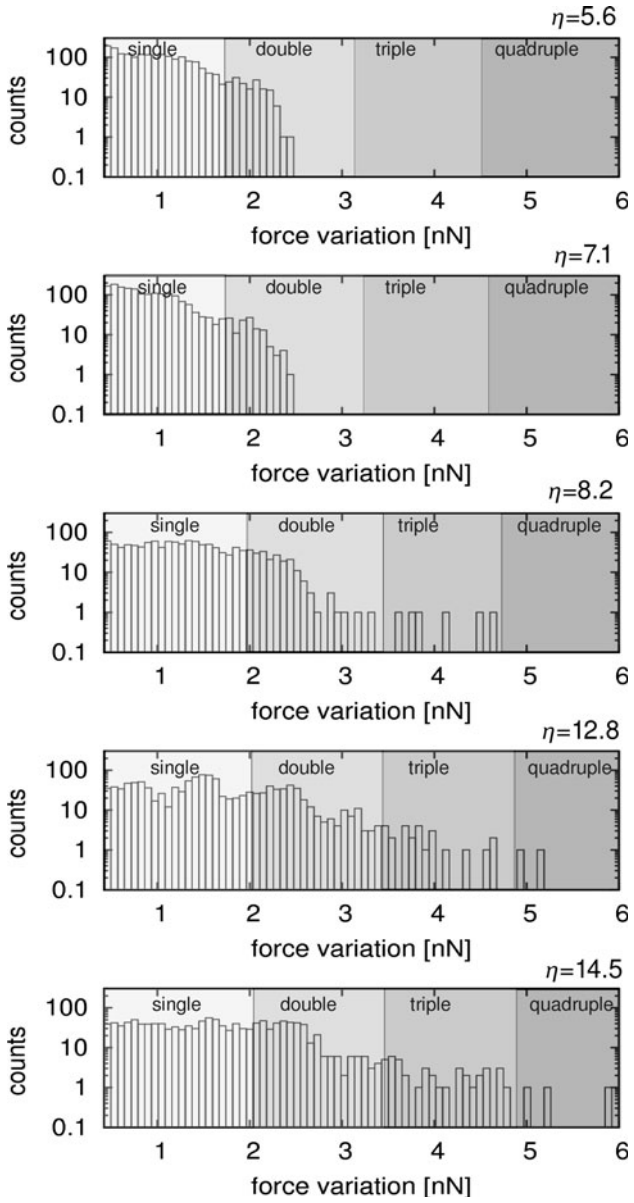

Fig. 5 From top to bottom: Room temperature histograms of force jumps obtained from measured lateral force maps for increasing loads corresponding to $\eta = 5.6$, 7.1, 8.2, 12.8, and 14.5. At the lower loads, only single and double slips could be revealed, wheras at the higher loads, genuine multiple slips were identified

which lowers the value of $F_{\max}$ [16, 17, 20]. Experimental histograms of force jumps are shown in Fig. 5. For the lowest loads, $\eta = 5.6$ and $\eta = 7.1$, mostly single slips with a small number of double slips occur. For higher loads, triple and quadruple slips could also be identified. Owing to the significant amount of instrumental noise in the experimental data, the histograms do not exhibit separated peaks like in Fig. 3, but rather a continuous distribution extending to higher ΔF_{L} at higher loads.

6 Conclusions

From a systematic visual comparison of experimental and simulated scans and histograms of ΔF_{L}, the following conclusions concerning the relative damping can be drawn for the last three plots in Fig. 5. When $\eta = 8.2$: $\gamma < 0.3 \cdot \gamma_{\mathrm{c}}$, when $\eta = 12.8$: $\gamma < 1.0 \cdot \gamma_{\mathrm{c}}$, and when $\eta = 14.5$: $\gamma < 1.5 \cdot \gamma_{\mathrm{c}}$. The successive appearance of higher multiple slips with increasing load can therefore be used to quantitatively estimate the ratio $\gamma/\gamma_{\mathrm{c}}$ in the range where an atomic-scale contact can be maintained without wear. Recalling that the load dependence of the critical damping γ_{c}, which in our model only comes from k_{eff}, is practically negligible, these conclusions imply that the load dependence of the lateral contact damping is weaker than that of the surface corrugation amplitude E_0, at least for the system under study. More generally, the lateral vibrations of an atomic-scale or nanometer-size contact with a clean crystal surface is not necessarily overdamped as often assumed. Upon increasing the load at room temperature, smooth crossovers from an underdamped regime to a critical damped state and finally to a slightly overdamped regime have been observed before wear sets in, previously on cleaved graphite [11], and now on the NaCl(001) surface.

Note finally that no systematic excitation of cantilever oscillations has been observed right after a lateral force jump, although several resonances of the cantilever in contact lie within the 3 MHz cutoff of our recording electronics [18]. This is expected if the effective mass of the contact is orders of magnitudes smaller than the masses of the tip as a whole and of the cantilever [19, 30]. The motion of the contact being much faster than the mechanical resonance modes of the cantilever in contact, no such modes can be effectively excited. Since the signals arising from the bending and torsion of the cantilever are filtered above the 3 MHz cutoff, the actual dynamics of the tip cannot be followed. It can nevertheless manifest itself at temperatures such that thermal activation induces frequent random contact slips over the time scale of cantilever torsional oscillations [30]. It is then necessary to consider the coupled dynamics of the contact and the cantilever [4, 18]. Whether the contact motion is underdamped [31] or overdamped [32] is then also of concern. Because multiple slips occur for relatively large values of η, hence E_0, we have neglected the dynamics of the cantilever in this study.

Acknowledgment We acknowledge the EUROCORE program FANAS, the Swiss National Center of Competence in Research on Nanoscale Science, and the Swiss National Science Foundation for financial support.

References

1. Mate, M., McClelland, G., Erlandsson, R., Chiang, S.: Atomic-scale friction of a tungsten tip on a graphite surface. Phys. Rev. Lett. **59**, 1942 (1987)
2. Fujisawa, S., Sugawara, Y., Ito, S., Mishima, S., Okada, T., Morita, S.: The two-dimensional stick-slip phenomenon with atomic resolution. Nanotechnology **4**, 138 (1993)
3. Tomlinson, G.: A molecular theory of friction. Philos. Mag. **7**, 905 (1929)
4. Johnson, K., Woodhouse, J.: Stick-slip motion in the atomic force microscope. Tribol. Lett. **5**, 155 (1998)
5. Socoliuc, A., Bennewitz, R., Gnecco, E., Meyer, E.: Transition from stick-slip to continuous sliding in atomic friction: entering a new regime of ultralow friction. Phys. Rev. Lett. **92**, 134301 (2004)
6. Gyalog, T., Gnecco, E., Meyer, E.: Stick-slip motion on the atomic scale. In: Gnecco, E., Meyer, E. (eds.) Fundamentals of Friction and Wear on the Nanoscale, pp. 101–115. Springer-Verlag, Berlin (2007)
7. Lifshits, A.I., Shluger, A.L.: Self-lubrication in scanning-force-microscope image formation on ionic surfaces. Phys. Rev. B **56**, 12482 (1997)
8. Fusco, C., Fasolino, A.: Velocity dependence of atomic-scale friction: a comparative study of the one- and two-dimensional Tomlinson model. Phys. Rev. B **71**, 045413 (2005)
9. Nakamura, J., Wakunami, S., Natori, A.: Double-slip mechanism in atomic-scale friction: Tomlinson model at finite temperatures. Phys. Rev. B **72**, 235415 (2005)
10. Tshiprut, Z., Zelner, S., Urbakh, M.: Temperature-induced enhancement of nanoscale friction. Phys. Rev. Lett. **102**, 136102 (2009)
11. Medyanik, S.N., Liu, W., Sung, I.-H., Carpick, R.: Predictions and observations of multiple slip modes in atomic-scale friction. Phys. Rev. Lett. **97**, 136106 (2006)
12. Persson, B.N.J.: Sliding Friction. Springer-Verlag, Berlin (2000)
13. Persson, B.N.J., Carbone, G., Samoilov, V.N., Siveback, I.M., Tartaglino, U., Volokitin, A.I., Yang, C.: Contact mechanics, friction and adhesion with application to quasicrystals. In: Gnecco, E., Meyer, E. (eds.) Fundamentals of Friction and Wear on the Nanoscale, pp. 269–306. Springer-Verlag, Berlin (2007)
14. Mo, Y., Turner, K.T., Szlufarska, I.: Friction laws at the nanoscale. Nature **457**, 1116 (2009)
15. Hölscher, H., Schwarz, U.D., Wiesendanger, R.: Simulation of a scanned tip on a NaF(001) surface in friction force microscopy. Europhys. Lett. **36**, 19 (1996)
16. Sang, Y., Dubé, M., Grant, M.: Thermal effects on atomic friction. Phys. Rev. B **87**, 174301 (2001)
17. Reimann, P., Evstigneev, M.: Description of atomic friction as forced brownian motion. N. J. Phys. **7**, 25 (2005)
18. Maier S., Sang Y., Filleter T., Grant M., Bennewitz R., Gnecco E., Meyer E.: Fluctuations and jump dynamics in atomic friction experiments. Phys. Rev. B **72**, 245418 (2005)
19. Socoliuc, A., Gnecco, E., Maier, S., Pfeiffer, O., Baratoff, A., Bennewitz, R., Meyer, E.: Atomic-scale control of friction by actuation of nanometer-sized contacts. Science **313**, 207 (2006)
20. Steiner, P., Roth, R., Gnecco, E., Baratoff, A., Maier, S., Glatzel, T., Meyer, E.: Two-dimensional simulation of superlubricity on NaCl and highly oriented pyrolytic graphite. Phys. Rev. B **79**, 045414 (2009)
21. Tshiprut, Z., Filippov, A., and Urbakh, M.: The effect of lateral vibrations on transport and friction in nanoscale contacts. Tribol. Int. **40**, 967 (2007)
22. Bilas, P., Romana, L., Bade, F., Delbe, K., Mansot, J.: Speed and atmosphere influences on nanotribological properties of $NbSe_2$. Tribol. Lett. **34**, 41 (2008)
23. Yabing, Q., Park, J.Y., Hendriksen, B.L.M., Ogletree, D.F., Salmeron, M.: Electronic contribution to friction on GaAs: an atomic force microscope study. Phys. Rev. B **77**, 184105 (2008)
24. Reinstädtler, M., Rabe, U., Scherer, V., Hartmann, U., Goldade, A., Bhushan, B., Arnold, W.: On the nanoscale measurement of friction using atomic-force microscope cantilever torsional resonances. Appl. Phys. Lett. **82**, 2604 (2003)
25. Gnecco, E., Bennewitz, R., Gyalog, T., Loppacher, Ch., Bammerlin, M., Meyer, E., Güntherodt, H.-J.: Velocity dependence of atomic friction. Phys. Rev. Lett. **84**, 1172 (2000)
26. Wyder, U., Baratoff, A., Meyer, E., Kantorovich, L.N., David, J., Maier, S., Filleter, T., Bennewitz, R.: Interpretation of atomic friction experiments based on atomistic simulations. J. Vac. Sci. Technol. B **25**, 1547 (2007)
27. Allen, M., Tildesley, D.: Computer Simulations of Liquids. Oxford Univeristy Press, Oxford (1991)
28. Howald, L., Meyer, E., Lüthi, R., Haefke, H., Overney, R., Rudin, H., Güntherodt, H.-J.: Multifunctional probe microscope for facile operation in ultrahigh vacuum. Appl. Phys. Lett. **63**, 117 (1993)
29. Schwarz, U., Koster, P., Wiesendanger, R.: Quantitative analysis of lateral force microscopy experiments. Rev. Sci. Instrum. **67**, 2560 (1996)
30. Krylov, S.Yu., Dijksman, J., van Loo, W., Frenken, J.M.: Stick-slip motion in spite of a slippery contact: Do we get what we see in atomic friction? Phys. Rev. Lett. **97**, 166103 (2006)
31. Krylov, S.Yu., Frenken, J.M.: Thermal contact delocalization in atomic scale friction: a multitude of friction regimes. N. J. Phys. **9**, 398 (2007)
32. Tshiprut, Z., Filippov, A., Urbakh, M.: Effect of tip flexibility on stick-slip motion in friction force microscopy experiments. J. Phys. Condens. Matter. **20**, 354002 (2008)